

Design and Stiffness Analysis of a Bio-inspired Soft Actuator with Bi-direction Tunable Stiffness Property

Jianfeng Lin, *Student Member, IEEE*, Ruikang Xiao, and Zhao Guo, *Member, IEEE*

Abstract—Modulating the stiffness of soft actuators is crucial for improving the efficiency of interaction with the environment. However, current stiffness modulation mechanisms are hard to achieve high lateral stiffness and a wide range of bending stiffness simultaneously. Here, we draw inspiration from the anatomical structure of the finger and propose a bi-directional tunable stiffness actuator (BTSA). BTSA is a soft-rigid hybrid structure that combines air-tendon hybrid actuation (ATA) and bone-like structures (BLS). We develop a corresponding fabrication method and a stiffness analysis model to support the design of BLS. The results show that the influence of the BLS on bending deformation is negligible, with a distal point distance error of less than 1.5 mm. Moreover, the bi-directional tunable stiffness is proved to be functional. The bending stiffness can be tuned by ATA from 0.23 N/mm to 0.70 N/mm, with a magnification of 3 times. The addition of BLS improves lateral stiffness up to 4.2 times compared with the one without BLS, and the lateral stiffness can be tuned decoupling within 1.2 to 2.1 times (e.g. from 0.35 N/mm to 0.46 N/mm when the bending angle is 45 deg). Finally, a four-BTSA gripper is developed to conduct horizontal lifting and grasping tasks to demonstrate the advantages of BTSA.

I. INTRODUCTION

Due to the adaptability, soft robotics have gained increasing attention in manipulation [1]–[3], rehabilitation [4], [5], grasping [6]–[12], and locomotion [13], [14]. On top of that, tunable stiffness further enhanced the performance by enabling large output force and stability while maintaining compliance and safety [15].

In this framework, active and semi-active stiffness regulation methods were proposed [15]. The active method is based on antagonistic actuation [16]–[19] like fluid actuation [16]. Varying stiffness by modulation of material property is the semi-active method [20]–[25] like material jamming [21]–[25]. However, there is still a gap for the soft actuator to have high lateral stiffness and large bending stiffness modulation range. As shown in Fig. 1a, the bending and lateral stiffness refer to the resistance to deformation by force on bending plane and force perpendicular to the bending plane, respectively.

For example, Jiang et al. [23] designed a chain-like granular jamming mechanism to enhance stiffness by controlling the pulling force to the mechanism. Although the

Research supported by the National Key Research and Development Program of China (No. 2023YFE0202100), the National Natural Science Foundation of China (Grant No. 51605339), and the Key Research and Development Program of Hubei Province (Grant NO. 2020BAB133). We are grateful to the Wuhan University Student Engineering Training and Innovation Practice Center for the venue and equipment support.

J. Lin, R. Xiao, and Z. Guo are at the School of Power and Mechanical Engineering, Wuhan University, Wuhan, 430072, China. Corresponding author to Zhao Guo (e-mail: guozhao@whu.edu.cn)

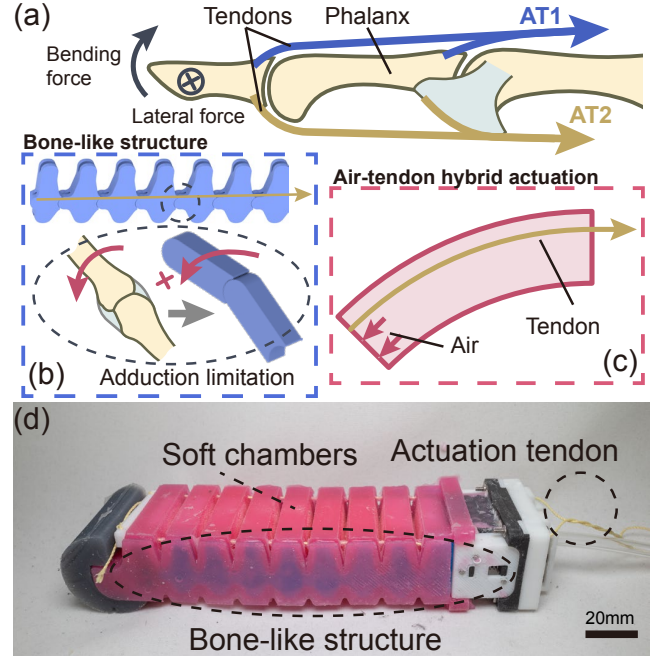


Fig. 1. The design concept of BTSA. (a) The anatomical feature of finger. (b) Description of adduction limitation of bone-like structure. (c) Description of air-tendon hybrid actuation. (d) The prototype of BTSA.

lateral stiffness can be ensured due to the thick jamming layer, it shows limited bending stiffness modulation range - little distal point position changed under different pulling forces. Contrary to that, the gas-ribbon-hybrid driven actuator proposed by Zhang et al. [26] shows a good compliance, but the lateral stiffness is small because the soft chamber and ribbon cannot provide an enhancement of lateral stiffness. Due to the low lateral stability, the soft gripper cannot lift objects horizontally like rigid grippers, which has a high grasping robustness according to [27].

In other studies [2], [28], [29], mechanical hinges were selected as an internal skeleton to reinforce lateral stiffness. However, the fixed connections limit the overall softness of the actuators. The micropump-activated jamming method [22] that demonstrates high stability can only become stiff at a single bending angle.

Therefore, in this paper, we propose a bi-directional tunable stiffness actuator (BTSA), as shown in Fig.1d. The bi-direction tunable stiffness property enables the actuator with high lateral stiffness and a wide range of bending stiffness. The BTSA consists of bone-like structure (BLS, Fig. 1b) and air-tendon hybrid actuation (ATA, Fig. 1c). The BLS draws

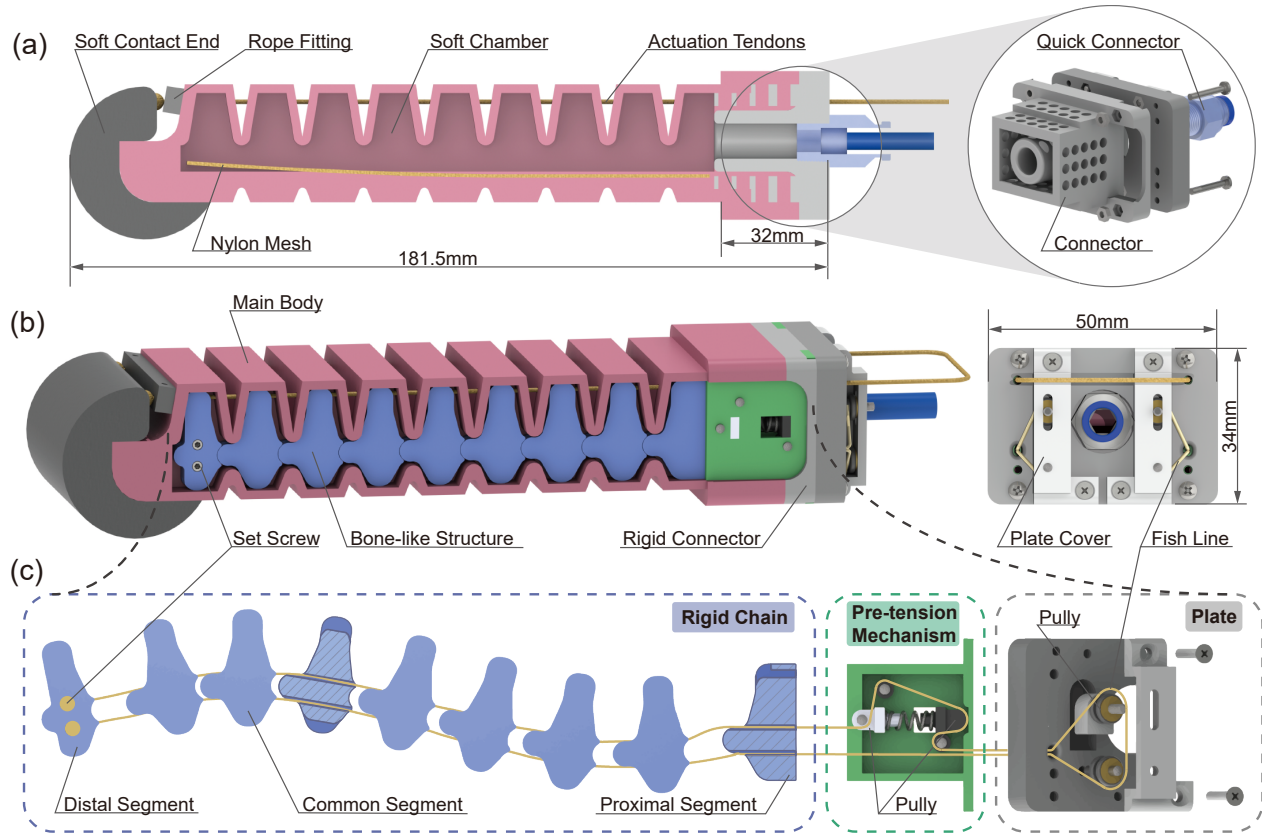


Fig. 2. The design details of the BTSA. (a) The sectional view of the main body and the details of the soft-rigid connection. (b) The overall structure (left) and back view (right) of BTSA. (c) The details of the bone-like structure.

inspiration from the morphological feature of the phalanx, simplifying the tuft and the base of phalanx into a semi-column. As Fig. 1b displays, all the segments which are connected by a rope can rotate freely while enhancing the lateral stiffness by the adduction limitation. By changing the pulling force to the rope, the lateral stiffness can be modulated decoupling. The air-tendon hybrid actuation (Fig. 1c) mimics antagonistic muscles of finger (AT1 and AT2 in Fig. 1a), achieving bending and stiffness control through air and tendon antagonism.

We detail the design and fabrication of BTSA. A simplified model for the lateral stiffness is presented. The design is further validated by the influence of the BLSs on deformation, bending and lateral stiffness, and grasping applications.

II. STRUCTURE DESIGN AND FABRICATION

A. Structure design

The main structure of BTSA, as Fig. 2b shows, is composed of three major parts, the main body, bone-like structures (BLSs), and the rigid connector. The two BLSs are attached to each side of the main body, connecting to the rigid connector.

Fig. 2a displays the sectional view of the main body and the details of the soft-rigid connection. The main body includes three components: a soft contact end, the soft chamber, and the actuation tendons. The soft chamber (Dragon

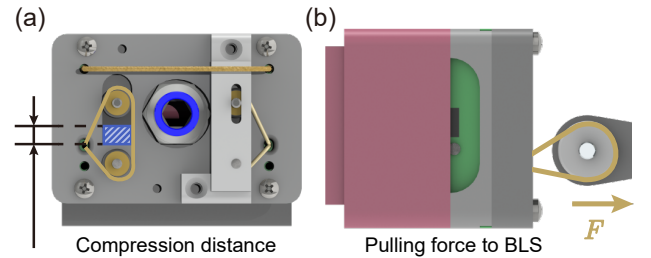


Fig. 3. Two methods to control the stiffness of BLS. (a) Add the PLA block (blue) to control the compression distance. (b) Connect the end of the rope to a pulley and then control the pulling force to BLS directly.

Skin 20, Smooth-On) is fabricated with a nylon mesh inserted to limit the elongation. The contact pad (Dragon Skin 30, Smooth-On) is designed to increase the fingertip force, glued on the front of the soft chamber [7]. The actuation tendons (Kevlar) cross through the holes in both sides of the actuator and tie to the rope fittings at the end of the actuator. These holes' centers are in the same plane as the symmetrical plane of BLS, which do not go through the chamber. The back of the soft chamber is cast into the connector. The quick connector is connected to the rigid connector through a pipe thread.

The design details of the bone-like structures are shown in Fig. 2c. There are three major parts in each BLS, rigid

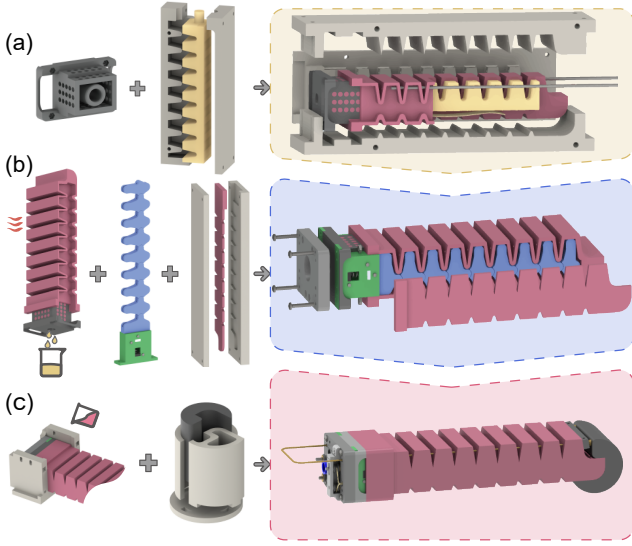


Fig. 4. The fabrication process of the proposed BTSA. (a) Fabricating the soft chamber. (b) Fit the BLSs. (c) Assemble other components.

chain, pre-tension mechanism, and plate, connected through a fishline goes across them. The fishline is fixed by two set screws in the distal segment and its path is shown in Fig. 2c in yellow. The bulge and concavity of the each segment are semi-cylindrical, and the holes are perforated along the tangent of the cylinder. The segments are designed as a bone to match the size of the actuator. The pre-tension mechanism (nylon) is to offer the pre-tightening force to BLS. The two pulleys (nylon) on each side of BLS provide a path to guide the fishline and form a closed-loop path. One of the pulleys is connected to the slider (PLA) placed in the chute of the backward plate (PLA).

As Fig. 3 shows, the lateral stiffness of BLS can be modulated in two ways: the passive way (Fig. 3a) by adding the blocks to change the position of the slider to regulate the pre-tightening force to BLS and the active way (Fig. 3b) by controlling the pulling force to BLS directly.

B. Fabrication

Firstly, fabricate the soft chamber. As Fig. 4a shows, the demolded wax core was fitted to the connector through the cylinder hole. The fluid silicone was poured into the pre-closed mold with the wax core, connector, and an embedded nylon mesh. Then, the soft chamber with a wax core in it was obtained after it was cured. In this case, the soft chamber would be one-piece molding and the porous sidewall of the connector reinforces the airtightness in the soft-rigid-connection boundary.

Then, fit the BLSs. As Fig. 4b displays, the soft chamber with a wax core was heated in the water bath to 85°C for 15 minutes. Squeezed out all the molten wax from the cylinder hole, the soft chamber was assembled with two BLSs and plate. Subsequently, two cover layers were cast and bonded with the soft chamber by uncured silicone.

In the end, assemble other components. As presented in Fig. 4c, the sealing layer of BTSA and the contact end were

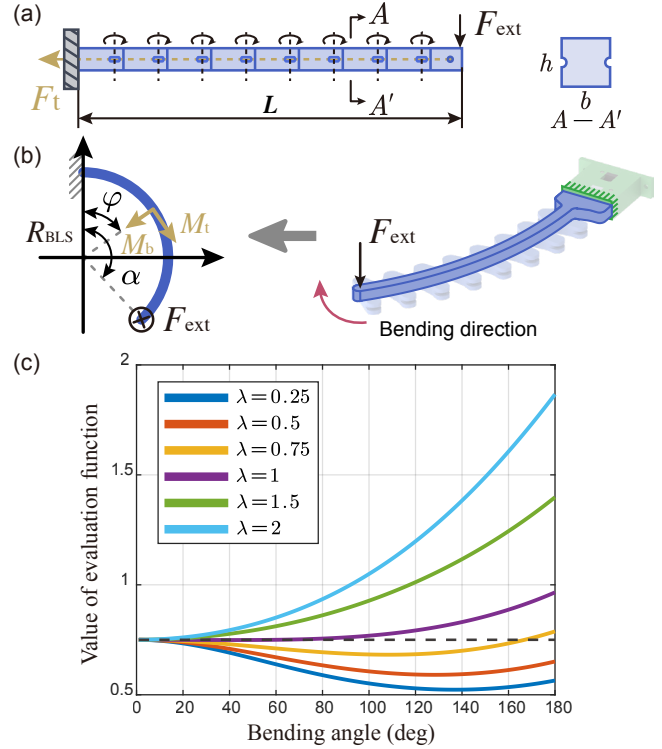


Fig. 5. Description of stiffness analysis of BLS. (a) Simplified schematic of BLS. (b) Simplified model of the curved cantilever beam. (c) The trend of stiffness with bending angle for different aspect ratios.

fabricated. After connecting the quick connector, gluing the contact end, and fitting the actuation tendon, the BTSA was fabricated.

III. STIFFNESS ANALYSIS

A. Bending stiffness

When the tendon in a relaxed, the actuator driven by pressuring will remain the high compliance. When the tightened tendons limits the bending of BTSA while the air pressure is still rising, The increased gas pressure will improve the bending stiffness.

B. Lateral stiffness

When BLS works normally, as Fig. 5a displays, the BLS can be considered as a multi-segment freely rotatable cantilever beam. The cross section of the beam is equivalent to the cross section of the bulge of segments. Adjacent segments are tightly bonded under the pulling force F_t of fishline.

When the destabilization does not occur, we assumed the pitch between each segment is small enough to be negligible. Hence, the BLS is modeled as a curved cantilever beam curving as the arc of a circle with centre angle α and radius R_{BLS} as Fig. 5b shows. The centre angle here is equal to the bending angle of BTSA. The axial length of the BLS is constant, so $R_{BLS}\alpha = L$.

For this equivalent beam, the contribution of shear force to the strain energy can be neglected. Therefore, the strain

energy U_{BLS} satisfying the following equation:

$$U_{BLS} = \frac{1}{EI} \int_0^\alpha M_b^2 R_{BLS} d\phi + \frac{1}{GI_p} \int_0^\alpha M_t^2 R_{BLS} d\phi \quad (1)$$

where M_t and M_b are torsion moment and bending moment, respectively, E is Young's modulus, I refers to the area moment of inertia, G is modulus of rigidity, and I_p represents polar moment of inertia. The G and I_p can be obtained from Poisson's ratio ν and aspect ratio λ of the beam:

$$\begin{cases} G = E / [2(1 + \nu)] \\ I_p = I(1 + \lambda^2) \end{cases} \quad (2)$$

According to Castigliano's second theorem, the stiffness can be derived as

$$k = \frac{4EI}{C^3} F(\alpha) \quad (3)$$

$$F(\alpha) = 1 / \left[A_{bending}(\alpha) + \frac{2(1 + \nu)A_{torsion}(\alpha)}{(1 + \lambda^2)} \right] \quad (4)$$

$A_{bending}(\alpha)$ and $A_{torsion}(\alpha)$ only vary with centre angle α , representing the influence of bending and torsion on displacement. Hence, $F(\alpha)$ is considered as an evaluation function to analyze the stiffness variation with centre angle α and aspect ratio λ .

The values of evaluation function are shown as Fig. 5c with that aspect ratio varies from 0.25 to 2 and Poisson's ratio is about 0.35 [30]. From Fig. 5c, the lateral stiffness increases with the bending when the aspect ratio is greater than 1. This is a desired property to ensure the lateral stability during bending. Meanwhile, according to equation (3), larger geometrical sizes means higher lateral stiffness. However, these parameters are limited by the size of soft chamber. Excessive parameters can cause undesired axial deformation. As a result, we chose 1 as the aspect ratio of BLS.

IV. EXPERIMENTS AND RESULTS

A. The influence of BLS on bending

Due to the friction between each segment, the BLS would might not work ideally that provides only the lateral stability enhancement but shows little influence on deformation. To test such influence, the second method (Fig. 3b) was chosen to control the lateral stiffness. Fig. 6a shows an intuitive comparison. When the pulling weight increased to 2 kg, the deformation was composed of several different segmented curvatures with a smaller curvature in the middle. This is different with the normal soft-actuator deformation with constant curvature like when pulling weight was 0 kg [6], [26], [31].

Further, we tested the position of distal point A to quantify this influence. BTSA was pressurized from 0 to 55 kPa with five groups of pulling forces. The center of the minimum circle which was calculated to cover the five recorder points was the average point. As Fig. 6b shows, with the increase of the pulling weights, all groups share the similar trends and the maximum error is within 1.5mm. This error is small enough to be ignored in most application cases.

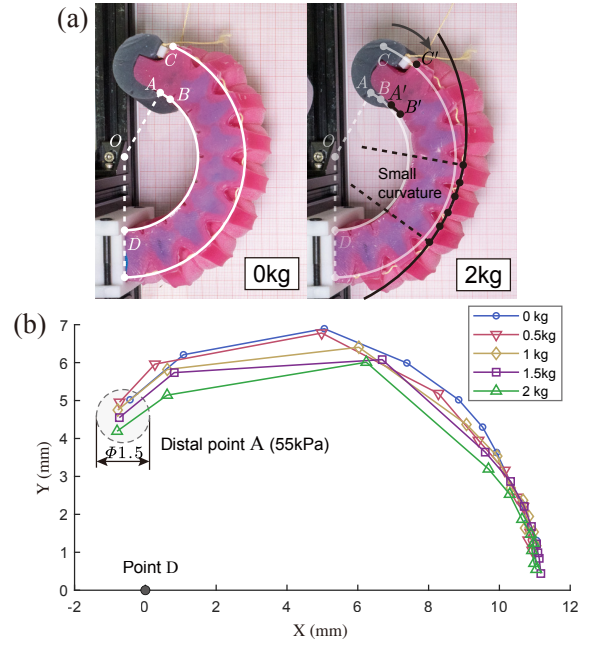


Fig. 6. Characterization of the influence of BLS on bending. (a) An intuitive comparison of bending between when the pulling force to BLSs is 0kg and 2kg. (b) Results of position of point A under pulling forces.

B. Bending stiffness

As shown in Fig. 7 a(i), a carbon fiber tube with 26mm diameter was connected to the force gauge. The sliding table was programmed to move 1mm rightward each time until the total distance reached 10mm and the pulling forces during this process would be recorded. For four groups of bending angle, four sets of incremental air pressures were set from the actuation pressure (the pressure when the actuator reaches certain bending angle) to maximum allowable pressure (85 kPa). The bending stiffness was calculated by the incremental ratio of the average force and displacement of three repeated experiments.

Fig. 7b lists all the test results. For all the four different bending angles, the stiffness was enhanced from 1.9 to 3.0 times, with a maximum stiffness of 0.70 N/mm, indicating that the stiffness in the bending direction is tuned successfully through proposed mechanism.

C. Lateral stiffness

The lateral stiffness was tested as Fig. 7a(ii) illustrates. The force gauge contacted by the end of the side of BTSA. Two weights were connected to each BLS through pulleys to change the pulling force by the second stiffness modulation method (Fig. 3b).

For BTSA, the lateral stiffness is influenced by both the input pressure and BLSs. Hence, the experiment has two variations: pulling weights to BLS and varying pressures. Five groups of weights 0kg, 0.5kg, 1kg, 1.5kg and 2kg and at least three groups of pressure at incremental steps of 10 kPa were conducted for five groups of bending angles. For comparison, the lateral stiffness for actuator without BLSs was also tested. The sliding table moved at a 1-mm interval

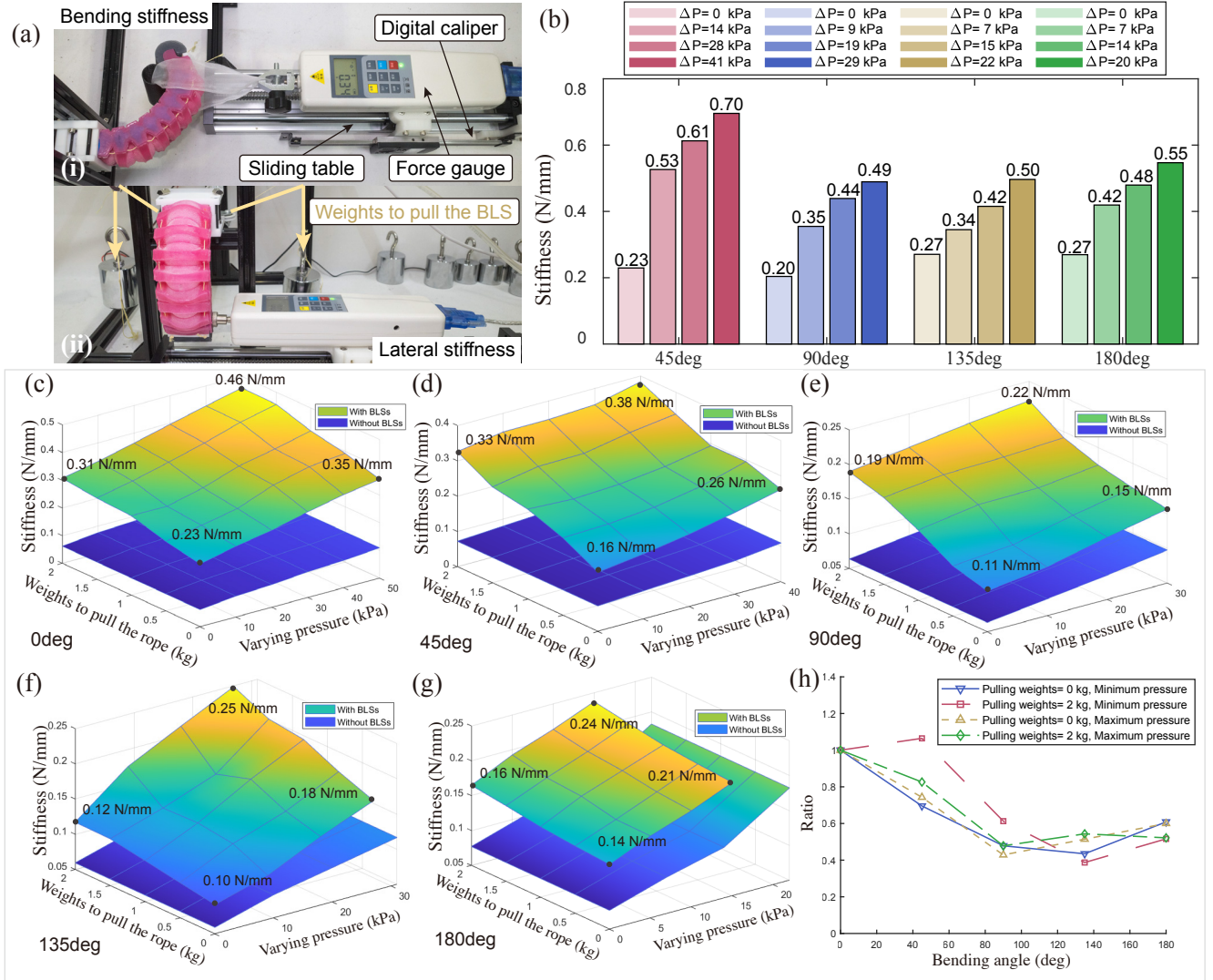


Fig. 7. The experimental platforms and results of stiffness testing. (a) The experiment platforms for (i) bending stiffness and (ii) lateral stiffness. (b) The testing results of bending stiffness. The testing results of lateral stiffness when bending angle is (c) 0 deg, (d) 45 deg, (e) 90 deg, (f) 135 deg, and (g) 180g. (h) The change of stiffness ratio with bending angle.

from 0 to 10mm to control the deflection. The stiffness was calculated after three repeated experiments.

All the results are shown from Fig. 7c to 7g. Comparisons between the lateral stiffness of BTSA with BLSs and without BLSs verifies the enhanced stiffness property of BLS. The maximum magnification reaches about 4.2 times when the bending angle is 0° . Meanwhile, for different input pressure, the lateral stiffness can be tuned by BLS within 1.2 to 2.1 times. These results proved that the lateral stiffness can be tuned decoupling successfully.

In addition, we choose four points in each angle and investigate the variation in lateral stiffness with angle to verify the analytical model. The ratios of stiffness relative to the value when the bending angle is 0 are calculated as Fig. 7h depicts. The graph shows that there has been a slight decrease followed by a rising, which does not match the design goal but is close to the trend of the analysis model when the aspect ratio λ is smaller than 1. The simplification

of the equivalent beam might contribute to the error since the segments are connected by elastic fishline.

D. Application cases

To demonstrate the performance of BLS, a four-BTSA gripper was designed. Each BLS was tightened to about 10N by the first stiffness regulation method (Fig. 3a). Firstly, several cross-weight and cross-scale tasks were successfully conducted, including an egg (47g, Fig. 8a), a tomato (261g, Fig. 8b), a watermelon (2221g, Fig. 8c), and a pipe (672, 200 mm diameters, Fig. 8d). Then, horizontal lifting was performed. The one with tightened BLSs could lift heavier targets (2358g) than the one without BLSs and shared similar displacement. These successful grasplings are the results of the bending and lateral stiffness adjustment.

V. CONCLUSIONS

In this work, we proposed a novel soft actuator design that can regulate bending and lateral stiffness, inspired by the

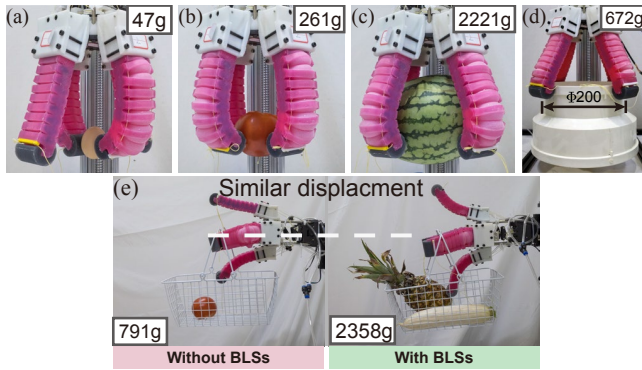


Fig. 8. The application cases of BTSA. Successful grasping tasks include (a) an egg, (b) a tomato, (c) a watermelon, and (d) a pipe. (e) Comparison between the gripper with BLSs and without BLSs.

anatomical structure of the finger. Our design offered a high lateral stiffness and a large range of bending stiffness, and we presented a theoretical stiffness analysis to support the design and analyse lateral stiffness. We also demonstrated that the influence of the rigid structure on deformation is negligible and verified the bi-directional stiffness regulation property through stiffness tests and application cases.

REFERENCES

- [1] H. Jiang, Z. Wang, Y. Jin, X. Chen, P. Li, Y. Gan, S. Lin, and X. Chen, "Hierarchical control of soft manipulators towards unstructured interactions," *The International Journal of Robotics Research*, vol. 40, no. 1, pp. 411–434, 2021.
- [2] C. Sozer, L. Paternò, G. Tortora, and A. Menciassi, "Pressure-driven manipulator with variable stiffness structure," in *2020 IEEE International Conference on Robotics and Automation (ICRA)*. IEEE, 2020, pp. 696–702.
- [3] S. Chen, Y. Pang, Y. Cao, X. Tan, and C. Cao, "Soft robotic manipulation system capable of stiffness variation and dexterous operation for safe human-machine interactions," *Advanced Materials Technologies*, vol. 6, no. 5, p. 2100084, 2021.
- [4] P. Polygerinos, Z. Wang, K. C. Galloway, R. J. Wood, and C. J. Walsh, "Soft robotic glove for combined assistance and at-home rehabilitation," *Robotics and Autonomous Systems*, vol. 73, pp. 135–143, 2015.
- [5] G. Gu, N. Zhang, H. Xu, S. Lin, Y. Yu, G. Chai, L. Ge, H. Yang, Q. Shao, X. Sheng *et al.*, "A soft neuroprosthetic hand providing simultaneous myoelectric control and tactile feedback," *Nature Biomedical Engineering*, pp. 1–10, 2021.
- [6] X. Liu, Y. Zhao, D. Geng, S. Chen, X. Tan, and C. Cao, "Soft humanoid hands with large grasping force enabled by flexible hybrid pneumatic actuators," *Soft Robotics*, vol. 8, no. 2, pp. 175–185, 2021.
- [7] S. Abondance, C. B. Teeple, and R. J. Wood, "A dexterous soft robotic hand for delicate in-hand manipulation," *IEEE Robotics and Automation Letters*, vol. 5, no. 4, pp. 5502–5509, 2020.
- [8] Y. Chen, S. Le, Q. C. Tan, O. Lau, F. Wan, and C. Song, "A reconfigurable hybrid actuator with rigid and soft components," in *2017 IEEE international conference on robotics and automation (ICRA)*. IEEE, 2017, pp. 58–63.
- [9] W. Park, S. Seo, and J. Bae, "Development of a hybrid gripper with soft material and rigid structures," in *2018 IEEE/RSJ International Conference on Intelligent Robots and Systems (IROS)*. IEEE, 2018, pp. 5930–5935.
- [10] L. Li, F. Xie, T. Wang, G. Wang, Y. Tian, T. Jin, and Q. Zhang, "Stiffness-tunable soft gripper with soft-rigid hybrid actuation for versatile manipulations," *Soft Robotics*, vol. 9, no. 6, pp. 1108–1119, 2022.
- [11] H. Wang, T. Howison, J. Hughes, A. Abdulali, and F. Iida, "Data-driven simulation framework for expressive piano playing by anthropomorphic hand with variable passive properties," in *2022 IEEE 5th International Conference on Soft Robotics (RoboSoft)*. IEEE, 2022, pp. 300–305.
- [12] K. Gilday, J. Hughes, and F. Iida, "Sensing, actuating, and interacting through passive body dynamics: A framework for soft robotic hand design," *Soft Robotics*, vol. 10, no. 1, pp. 159–173, 2023.
- [13] Y. Zhang, D. Yang, P. Yan, P. Zhou, J. Zou, and G. Gu, "Inchworm inspired multimodal soft robots with crawling, climbing, and transitioning locomotion," *IEEE Transactions on Robotics*, 2021.
- [14] A. Rafsanjani, Y. Zhang, B. Liu, S. M. Rubinstein, and K. Bertoldi, "Kirigami skins make a simple soft actuator crawl," *Science Robotics*, vol. 3, no. 15, p. eaar7555, 2018.
- [15] M. Manti, V. Cacucciolo, and M. Cianchetti, "Stiffening in soft robotics: A review of the state of the art," *IEEE Robotics & Automation Magazine*, vol. 23, no. 3, pp. 93–106, 2016.
- [16] M. A. Robertson, H. Sadeghi, J. M. Florez, and J. Paik, "Soft pneumatic actuator fascicles for high force and reliability," *Soft robotics*, vol. 4, no. 1, pp. 23–32, 2017.
- [17] Y. She, J. Chen, H. Shi, and H.-J. Su, "Modeling and validation of a novel bending actuator for soft robotics applications," *Soft Robotics*, vol. 3, no. 2, pp. 71–81, 2016.
- [18] M. Manti, T. Hassan, G. Passetti, N. D'Elia, C. Laschi, and M. Cianchetti, "A bioinspired soft robotic gripper for adaptable and effective grasping," *Soft Robotics*, vol. 2, no. 3, pp. 107–116, 2015.
- [19] J. Li, L. Zu, G. Zhong, M. He, H. Yin, and Y. Tan, "Stiffness characteristics of soft finger with embedded sma fibers," *Composite Structures*, vol. 160, pp. 758–764, 2017.
- [20] C. Majidi and R. J. Wood, "Tunable elastic stiffness with micro-confined magnetorheological domains at low magnetic field," *Applied Physics Letters*, vol. 97, no. 16, p. 164104, 2010.
- [21] J. Shintake, B. Schubert, S. Rosset, H. Shea, and D. Floreano, "Variable stiffness actuator for soft robotics using dielectric elastomer and low-melting-point alloy," in *2015 IEEE/RSJ International Conference on Intelligent Robots and Systems (IROS)*. IEEE, 2015, pp. 1097–1102.
- [22] H. H. Huynh, D. Han, K. Yoshida, M. De Volder, and J.-w. Kim, "Soft actuator with switchable stiffness using a micropump-activated jamming system," *Sensors and Actuators A: Physical*, vol. 338, p. 113449, 2022.
- [23] Y. Jiang, D. Chen, C. Liu, and J. Li, "Chain-like granular jamming: a novel stiffness-programmable mechanism for soft robotics," *Soft robotics*, vol. 6, no. 1, pp. 118–132, 2019.
- [24] S. Jadhav, M. R. A. Majit, B. Shih, J. P. Schulze, and M. T. Tolley, "Variable stiffness devices using fiber jamming for application in soft robotics and wearable haptics," *Soft Robotics*, vol. 9, no. 1, pp. 173–186, 2022.
- [25] Y. Wei, Y. Chen, T. Ren, Q. Chen, C. Yan, Y. Yang, and Y. Li, "A novel, variable stiffness robotic gripper based on integrated soft actuating and particle jamming," *Soft Robotics*, vol. 3, no. 3, pp. 134–143, 2016.
- [26] X. Zhang, J. Yan, and J. Zhao, "A gas-ribbon-hybrid actuated soft finger with active variable stiffness," *Soft Robotics*, vol. 9, no. 2, pp. 250–265, 2022.
- [27] S. Makita and K. Makihara, "Homogeneous quantitative measure of caging grasps with both geometrical and mechanical constraints," *2019 19th International Conference on Control, Automation and Systems (ICCAS)*, pp. 311–316, 2019.
- [28] M. Su, R. Xie, Y. Zhang, X. Kang, D. Huang, Y. Guan, and H. Zhu, "Pneumatic soft actuator with anisotropic soft and rigid restraints for pure in-plane bending motion," *Applied Sciences*, vol. 9, no. 15, 2019. [Online]. Available: <https://www.mdpi.com/2076-3417/9/15/2999>
- [29] J. Zhu, Z. Chai, H. Yong, Y. Xu, C. Guo, H. Ding, and Z. Wu, "Bioinspired multimodal multipose hybrid fingers for wide-range force, compliant, and stable grasping," *Soft Robotics*, vol. 10, no. 1, pp. 30–39, 2023.
- [30] D. D. Wright-Charlesworth, D. M. Miller, I. Miskioglu, and J. A. King, "Nanoindentation of injection molded pla and self-reinforced composite pla after in vitro conditioning for three months," *Journal of Biomedical Materials Research Part A*, vol. 74A, no. 3, pp. 388–396, 2005. [Online]. Available: <https://onlinelibrary.wiley.com/doi/abs/10.1002/jbm.a.30353>
- [31] J. H. Low, J. Goh, N. Cheng, P. Khin, Q. Han, and C.-H. Yeow, "A bidirectional 3d-printed soft pneumatic actuator and graphite-based flex sensor for versatile grasping," in *2020 IEEE International Conference on Robotics and Automation (ICRA)*. IEEE, 2020, pp. 7979–7985.